Optics Letters

Hybrid coupling enhances photoluminescence of monolayer MoS_2 on plasmonic nanostructures

Wen-Bo Shi,[1] Lei Zhang,[1] Di Wang,[2] Rui-Li Zhang,[1] Yingying Zhu,[1] Li-Heng Zhang,[1] Ruwen Peng,[1,4] Wenzhong Bao,[3] Ren-Hao Fan,[1] and Mu Wang[1,5]

[1]National Laboratory of Solid State Microstructures, School of Physics, and Collaborative Innovation Center of Advanced Microstructures, Nanjing University, Nanjing 210093, China
[2]Institute of Functional Crystals, Tianjin University of Technology, Tianjin 300384, China
[3]School of Microelectronics, Fudan University, 220 Handan Road, Shanghai 200433, China
[4]e-mail: rwpeng@nju.edu.cn
[5]e-mail: muwang@nju.edu.cn

Received 12 June 2018; accepted 26 July 2018; posted 30 July 2018 (Doc. ID 334991); published 20 August 2018

The efficiency of photoluminescence (PL) of transition-metal dichalcogenides (TMDCs) significantly influences their practical applications in optoelectronic devices. In this work, we study multiple coupling among excitons, surface plasmons, and optical modes, and their effects on PL of monolayer MoS_2 atop plasmonic nanohole arrays. Under the illumination of visible light, strong intensity enhancement of PL from monolayer MoS_2 is observed in the system. We further demonstrate that there exist excitons induced from MoS_2, localized and propagating surface plasmons excited from nanoholes, and optical modes related to the incident laser. And hybrid coupling of those modes significantly improves the PL signals and also lightens the PL images of monolayer MoS_2. This work provides a unique way to improve the emission of monolayer TMDCs. The atomically thin TMDCs coupled to plasmonic metamaterials are also promising for advanced applications such as ultrathin integrated light-emission diodes, photodetection, and nanolasers.

OCIS codes: (300.2530) Fluorescence, laser-induced; (250.5230) Photoluminescence; (250.5403) Plasmonics; (310.6628) Subwavelength structures, nanostructures.

https://doi.org/10.1364/OL.43.004128

Monolayer transition-metal dichalcogenides (TMDCs), such as MoS_2, WSe_2, and WS_2, have attracted much attention because of their atomically thin thickness, direct bandgap, and strong exciton binding energy [1–3]. These unique properties have inspired versatile applications in electronics and photonics, such as light-emitting diodes (LEDs), valley-selective circular dichroism, and nanolasers [4–16]. The efficiency of photoluminescence (PL) of TMDCs significantly influences their practical applications in optoelectronic devices. It is known that the PL from MoS_2 can be tuned by different methods such as applying gate voltage to accumulate electrons or holes [17–19], using hybrid heterostructures to affect carrier recombination [20–22], and also chemical doping to change the carrier density [23,24]. Physically, these methods can enhance the PL by tuning the photogenerated carriers in MoS_2. Besides, there is another approach to achieve strong PL, i.e., enhancing the light–matter interaction via photonic crystals [25,26] or plasmonic metamaterials.

As we know, plasmonic metamaterials have been studied extensively because of their subwavelength-confined optical modes with highly enhanced electric fields [27–31]. These properties have inspired potential applications on optoelectronics [32–36]. Recently, integrated plasmonic systems with ultracompact integration have attracted much attention [37,38]. MoS_2 is a promising candidate when combined with plasmonic structures for advanced optoelectronic applications. Actually the coupling between different modes and strong light–matter interaction can be achieved in MoS_2 when combined with plasmonic nanostructures, where the PL emission can be significantly improved [39–43]. For example, plasmonic nanoantennas or nanorods are used to enhance the laser absorption to achieve a larger PL signal, where the surface plasmons can couple to the optical mode [44–47]. Moreover, in many plasmonic structures, surface plasmons are used to couple to the exciton modes of MoS_2, and then the coupling can enhance the PL efficiency [48–52]. Now that the improvement of PL has been achieved by either enhancing the laser absorption or coupling the exciton modes to recycling PL energy, it becomes possible to further simultaneously improve the PL from MoS_2 by enhancing the absorption of laser and coupling exciton modes in a hybrid MoS_2–plasmonic system.

In this work, we focus on the hybrid coupling between excitons, surface plasmons, and optical modes, and its effects on PL of monolayer MoS_2 atop of the plasmonic nanohole arrays. We design nanohole arrays in a silver film with various periods. The resonance modes in the structures, including the localized surface plasmon (LSP) mode and propagated surface plasmon (PSP) mode, are affected by the array periods. Then, we choose certain periodic structures that can couple to the excitation laser or a certain exciton mode of MoS_2. We achieve strong PL

intensity enhancement in the MoS_2-hole array hybrid system. Furthermore, we combine different periodic structures to excite hybrid modes to improve the enhancement. Hybrid coupling among those modes can be acquired, and as a result, PL emission can be efficiently enhanced. Our work provides unique methods of PL enhancement by hybrid modes in plasmonic nanostructures.

We first fabricate samples by depositing a 100-nm-thick silver layer by magnetron sputtering on a Si substrate and then etch the hole arrays by the focused ion beam (FIB, Helios Nanolab 600i) technique. Scanning electron microscopy (SEM) images of the etched arrays are shown in Figs. 1(a) and 1(b). We then show the plasmonic modes excited in the hole arrays in the silver film through the reflection spectra of structures with periods of 450 nm (S1) and 650 nm (S2), as shown in Figs. 1(c) and 1(d), respectively. The spectra calculated by the finite-difference time-domain (FDTD) method (Lumerical FDTD Solution 8.0.1) are plotted together with experimental data in Figs. 1(c) and 1(d), and we find these data are fitted to each other very well. In the reflection spectra of S1 shown in Fig. 1(c), a distinct dip can be found at 514 nm, which is intentionally matched to the excitation laser when we design the structure. We have marked this mode in S1 as mode one (M1). In the reflection spectra of S2 in Fig. 1(d), two modes arise: one mode is around 514 nm (M2) that is similar to M1 but lower in amplitude, and the other is around 670 nm (M3). We also plot the PL spectrum of monolayer MoS_2 in Fig. 1(d), and we find that M3 overlaps with the PL peak of MoS_2. As shown in Fig. 1(d), the PL spectrum of MoS_2 can be fitted by two Gaussian peaks that separately account for contributions from the A exciton and the B exciton. We can find that M3 exactly overlaps with the peak from the A exciton. So, we can find that in S2 these surface plasmons can couple to the optical mode and A exciton mode, respectively.

Then we attempt to analyze these modes by investigating the electric field distributions from calculations. Electric field distributions in both the horizontal ($x-y$) and vertical ($x-z$) sections of these modes (M1–M3) are obtained, as shown in Fig. 1(e). From the distributions, we can categorize these modes in two classes, namely LSP modes excited around the hole with a highly enhanced electric field (M1, M2) and PSP modes that can propagate along the silver surface (M3). We find that all these modes can highly enhance the electric field not only at the surface but also in the vertical area (over 20 nm from the silver surface). This result implies that in the hybrid system, the electric field around MoS_2 can be enhanced greatly when these modes are excited, and the enhanced electric field can improve the PL efficiency of MoS_2.

Now we examine the PL of monolayer MoS_2 on several plasmonic nanohole arrays. As shown in Fig. 2(a), a 20-nm-thick SiO_2 layer was first deposited on the silver nanostructure as an isolation layer. Monolayer MoS_2 flakes grown by the chemical vapor deposition (CVD) method [53] were then transferred on the fabricated silver nanohole arrays. For example, Fig. 2(b) shows a MoS_2 triangular domain covering the Ag nanohole array (S1) with a period of 450 nm, and Fig. 2(c) shows the SEM image of the same sample. We have also carried out the PL measurements of monolayer MoS_2 on the Ag nanohole array (S2) with a period of 650 nm. As shown in Fig. 2(d), both PL spectra (left) and Raman spectra (right) excited by a 514 nm laser are collected from S1, S2, and the bare area on Ag and SiO_2 (without the patterned holes) of the MoS_2 flake. Comparing these three cases, we find that the PL signal can be significantly enhanced when MoS_2 flakes are placed on plasmonic structures. Also the intensity enhancement from S1 is stronger than that from S2, which can be attributed to the highly enhanced electric field in M1 as obviously illustrated in Fig. 1(e). In order to show the PL enhancement clearly, the PL and Raman signal mappings of the sample are measured, as shown in Figs. 2(e) and 2(f). It is obvious that enhancement occurs when MoS_2 covers the nanohole array. As discussed above, with LSP or PSP modes excited in hole array structures, hybrid coupling among surface plasmons, optical modes, and exciton modes can induce the strong intensity enhancement of both PL and Raman signals.

Such PL enhancement can be attributed to hybrid coupling of different modes. It becomes possible to achieve PL enhancement by combining different plasmonic structures to excite hybrid plasmonic modes. Therefore, we try to enhance the PL signal further by combining two structures with a period of 450 nm in the transverse (x) direction and a period of 650 nm in the longitudinal (y) direction (S3), as shown in Fig. 3(a).

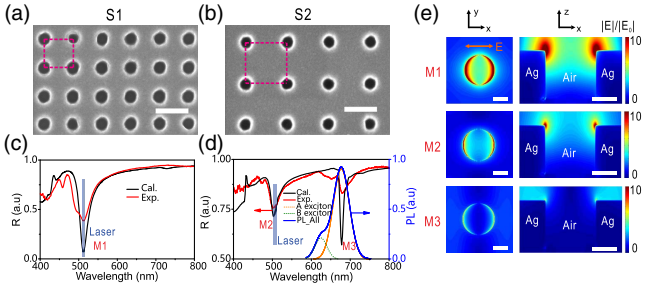

Fig. 1. SEM images of the hole arrays in silver film with period of (a) 450 nm (S1) and (b) 650 nm (S2). The scale bar is 500 nm. (c) Reflection spectra of S1 including both experimental and calculated data. (d) Reflection spectra of S2 (left axis) and PL spectrum of monolayer MoS_2 (right axis). The PL spectrum can be fitted by two Gaussian peaks. (e) Electric field distributions of optical modes excited in S1 and S2. The scale bar is 100 nm in all subfigures. The orange double-headed arrow shows schematically the polarization direction of the electric field.

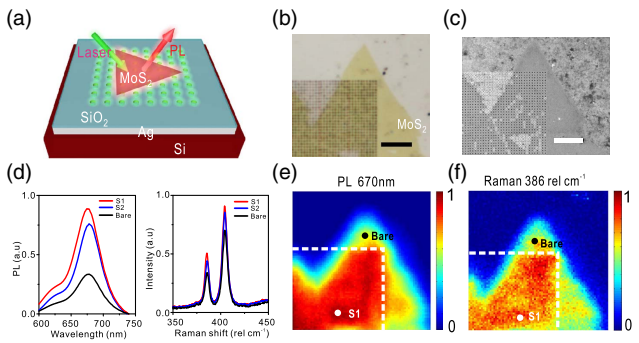

Fig. 2. (a) Schematic view of a sample fabricated with MoS_2 flakes transferred onto the hole array. (b, c) Photograph and SEM image of the sample with MoS_2 flakes placed on S1. The scale bar is 5 μm. (d) Left, PL spectra of MoS_2 samples with S1, S2, and without any structure (Bare). Right, Raman spectra of these samples. (e, f) PL and Raman mappings of the sample in (b). White dot (S1) and black dot (Bare) show the locations of the PL and Raman spectra shown in (d).

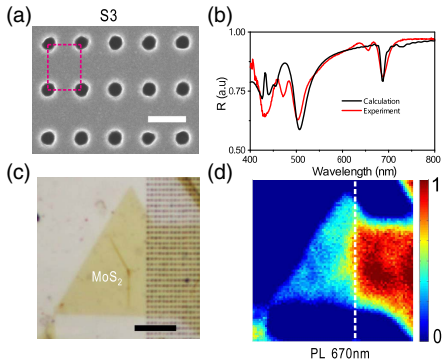

Fig. 3. SEM image of the hole array with a period of 450 nm in the transverse direction and 650 nm in the longitudinal direction (S3); the scale bar is 500 nm. (b) Reflection spectra of S3. (c) Photograph of the fabricated sample with MoS_2 flakes placed on S3; the scale bar is 5 μm. (d) PL mapping of the sample.

In the reflection spectrum of S3 in Fig. 3(b), we can see two obvious modes. The first dip around 514 nm is clearly deeper than that of M2 because it originates from both M1 in S1 and M2 in S2; meanwhile, the second dip originating from M3 is conserved. So indeed hybrid modes can be excited in the S3 structure. A photograph of this sample is shown in Fig. 3(c), and PL mapping of the same sample is shown in Fig. 3(d). We can clearly see a distinct contrast of PL intensity between samples with and without the hole array in the PL mapping. It is apparent that S3 can strongly enhance the PL of MoS_2.

The PL spectra measured from different structures (S1–S3) are shown in Fig. 4(a). The intensity enhancement from S3 is the largest among all structures, which indicates that the hybrid modes excited in S3 effectively enhance the PL. Another noticeable phenomenon is that the A exciton peak (around 670 nm) from S3 is clearly higher than that from S1, while the B exciton peak (around 620 nm) from S3 is approximately equal to that from S1. This suggests that different enhancements between A and B excitons can be acquired in these structures. To clarify this difference between A and B excitons, the PL enhancement of A exciton and B exciton from different structures (S1, S2, S3) is shown in Fig. 4(b). The intensity enhancement of PL can be evaluated by integrating the intensity

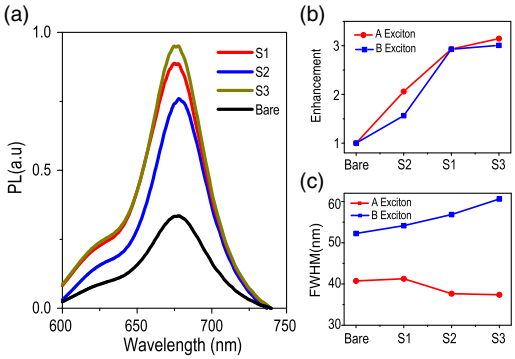

Fig. 4. (a) PL spectra of MoS_2 with S1, S2, S3, and without any structure (Bare). (b) Enhancement of PL signal from A exciton and B exciton. (c) FWHM of A exciton and B exciton peaks in different structures.

of the A exciton peak or B exciton peak [fitted from the entire PL spectra, as shown in Fig. 1(d)], and normalizing it to that in bare structure. The enhancement factor is defined as the ratio of the PL intensity from A exciton or B exciton on the hole structures to that on bare structure, which indicates the PL enhancement from the hole structure. We can see that the differences between A and B excitons occur only in the structures (S2, S3) that can excite the PSP mode. On the contrary, in structure S1, the enhancements of A and B excitons are not different. The reason is that the LSP mode only couples with the optical mode from the laser and enhances laser absorption, but the PSP mode couples to A exciton and enhances its emission. Interestingly the PL enhancement effect in this system can be further improved by several ways, such as decreasing the thickness of the SiO_2 layer or reducing the defects in MoS_2 via annealing in vacuum. We also investigate the full-width at half-maximum (FWHM) of A and B exciton peaks, as shown in Fig. 4(c). The FWHMs of B exciton peak in S1, S2, and S3 are all larger than that in the bare structure. However, the FWHMs of A exciton peak in S1, S2, and S3 are in two different cases, i.e., in S1, the FWHM is larger than that in the bare structure and in S2 and S3, the FWHMs are smaller than that in the bare structure. Therefore, with the PSP mode excited at 670 nm, S2 and S3 can selectively enhance the A exciton mode and decrease the FWHM of the A exciton peak.

To visualize the PL enhancement in our designed structures, we directly capture PL images by a charge-coupled device (CCD) with laser filters. Figures 5(a)–5(d) show the PL images from monolayer MoS_2 without any other structure (bare), with S1, S2, and S3, respectively, where the power of the excitation laser is the same in all conditions. We can compare the emission intensity and the emission area of PL signals in these images to find the influence of excited modes from different structures. It is interesting to see that the PL signal in Fig. 5(b) is much stronger than that in Fig. 5(a). This phenomenon exactly conforms to the LSP modes in S1, where the LSP modes exhibit highly enhanced fields around the holes. While the PL area in Fig. 5(c) is much broader compared to Fig. 5(a), and this conforms to PSP modes in S2 because the PSP modes can propagate to broader areas. Since both modes are conserved in S3, the PL image in Fig. 5(d) exhibits a brighter and broader spot. These PL images can directly show the consequences of different modes excited in our designed structures and verify that enhancement of PL originates from the hybrid plasmonic modes.

In conclusion, we have demonstrated that hybrid coupling among excitons, surface plasmons, and optical modes happens

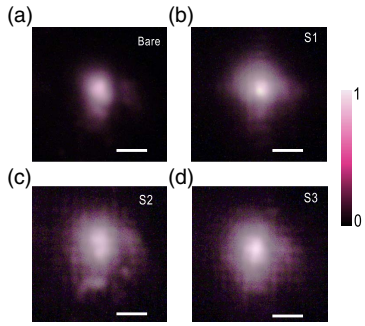

Fig. 5. PL images of MoS_2 samples (a) without any structure, (b) with S1, (c) with S2, and (d) with S3. The scale bar is 3 μm.

in combined plasmonic nanostructures with monolayer MoS_2. The hybrid coupling has significantly enhanced the PL of monolayer MoS_2. Under the illumination of visible light, the excitons from MoS_2, the LSPs, and PSPs excited in the metallic nanostructure and the optical modes related to the incident laser are all coupled together. Consequently, significant intensity enhancement of the PL has been achieved in the system. Currently the experiments are carried out in monolayer MoS_2 systems, yet similar results can be expected in other TMDCs. Therefore, the atomically thin TMDCs combined with plasmonic metamaterials are promising for advanced applications such as ultrathin integrated LEDs, photodetectors, and nanolasers.

Funding. National Key R&D Program of China (2017YFA0303702); National Natural Science Foundation of China (NSFC) (11634005, 51472123, 61475070, 11474157, 11674155, 11604143, 11621091); "333 Project" from Jiangsu Province (BRA2016350).

REFERENCES

1. K. F. Mak, C. Lee, J. Hone, J. Shan, and T. F. Heinz, Phys. Rev. Lett. **105**, 136805 (2010).
2. K. F. Mak, K. He, C. Lee, G. H. Lee, J. Hone, T. F. Heinz, and J. Shan, Nat. Mater. **12**, 207 (2013).
3. A. Chernikov, T. C. Berkelbach, H. M. Hill, A. Rigosi, Y. L. Li, O. B. Aslan, D. R. Reichman, M. S. Hybertsen, and T. F. Heinz, Phys. Rev. Lett. **113**, 076802 (2014).
4. Z. Yin, H. Li, H. Li, L. Jiang, Y. Shi, Y. H. Sun, G. Lu, Q. Zhang, X. D. Chen, and H. Zhang, ACS Nano **6**, 74 (2011).
5. D. Xiao, G. B. Liu, W. Feng, X. Xu, and W. Yao, Phys. Rev. Lett. **108**, 196802 (2012).
6. G. Kioseoglou, A. T. Hanbicki, M. Currie, A. L. Friedman, D. Gunlycke, and B. T. Jonker, Appl. Phys. Lett. **101**, 221907 (2012).
7. H. P. Komsa and A. V. Krasheninnikov, Phys. Rev. B **86**, 241201 (2012).
8. E. S. Reich, Nature **497**, 422 (2013).
9. Q. Wang, S. Ge, X. Li, J. Qiu, Y. Ji, J. Feng, and D. Sun, ACS Nano **7**, 11087 (2013).
10. T. C. Berkelbach, M. S. Hybertsen, and D. R. Reichman, Phys. Rev. B **88**, 045318 (2013).
11. M. L. Tsai, S. H. Su, J. K. Chang, D. S. Tsai, C. H. Chen, C. I. Wu, L. J. Li, L. J. Chen, and J. H. He, ACS Nano **8**, 8317 (2014).
12. Y. H. Chang, W. Zhang, Y. Zhu, Y. Han, J. Pu, J. K. Chang, W. T. Hsu, J. K. Huang, C. L. Hsu, M. H. Chiu, T. Takenobu, H. Li, C. I. Wu, W. H. Chang, A. T. S. Wee, and L. J. Li, ACS Nano **8**, 8582 (2014).
13. F. Withers, O. D. P. Zamudio, A. Mishchenko, A. P. Rooney, A. Gholinia, K. Watanabe, T. Taniguchi, S. J. Haigh, A. K. Geim, A. I. Tartakovskii, and K. S. Novoselov, Nat. Mater. **14**, 301 (2015).
14. K. J. Tielrooij, L. Piatkowski, M. Massicotte, A. Woessner, Q. Ma, Y. Lee, K. S. Myhro, C. N. Lau, P. J. Herrero, N. F. van Hulst, and F. H. L. Koppens, Nat. Nanotechnol. **10**, 437 (2015).
15. S. Wu, S. Buckley, J. R. Schaibley, L. F. Feng, J. Q. Yan, D. G. Mandrus, F. Hatami, W. Yao, J. Vuckovic, A. Majumdar, and X. D. Xu, Nature **520**, 69 (2015).
16. Y. Ye, Z. J. Wong, X. Lu, X. J. Ni, H. Y. Zhu, X. H. Chen, Y. Wang, and X. Zhang, Nat. Photonics **9**, 733 (2015).
17. Y. J. Zhang, T. Oka, R. Suzuki, J. T. Ye, and Y. Iwasa, Science **344**, 725 (2014).
18. J. S. Ross, P. Klement, A. M. Jones, N. J. Ghimire, J. Q. Yan, D. G. Mandrus, T. Taniguchi, K. Watanabe, K. Kitamura, W. Yao, D. H. Cobden, and X. D. Xu, Nat. Nanotechnol. **9**, 268 (2014).
19. Z. Li, S. W. Chang, C. C. Chen, and S. B. Cronin, Nano Res. **7**, 973 (2014).
20. K. Roy, M. Padmanabhan, S. Goswami, T. P. Sai, G. Ramalingam, S. Raghavan, and A. Ghosh, Nat. Nanotechnol. **8**, 826 (2013).
21. C. Huang, S. Wu, A. M. Sanchez, J. J. P. Peters, R. Beanland, J. S. Ross, P. Rivera, W. Yao, D. H. Cobden, and X. D. Xu, Nat. Mater. **13**, 1096 (2014).
22. P. Rivera, J. R. Schaibley, A. M. Jones, J. S. Ross, S. F. Wu, G. Aivazian, P. Klement, K. Seyler, G. Clark, N. J. Ghimire, J. Q. Yan, D. G. Mandrus, W. Yao, and X. D. Xu, Nat. Commun. **6**, 6242 (2015).
23. S. Mouri, Y. Miyauchi, and K. Matsuda, Nano Lett. **13**, 5944 (2013).
24. H. Nan, Z. Wang, W. Wang, Z. Liang, Y. Lu, Q. Chen, D. W. He, P. H. Tan, F. Miao, X. R. Wang, J. L. Wang, and Z. H. Ni, ACS Nano **8**, 5738 (2014).
25. X. Gan, Y. Gao, K. F. Mak, X. Yao, R. J. Shiue, A. van der Zande, M. E. Trusheim, F. Hatami, T. F. Heinz, J. Hone, and D. Englund, Appl. Phys. Lett. **103**, 181119 (2013).
26. S. Wu, S. Buckley, A. M. Jones, J. S. Ross, N. J. Ghimire, J. Yan, D. G. Mandrus, W. Yao, F. Hatami, J. Vučković, A. Majumdar, and X. D. Xu, 2D Materials **1**, 011001 (2013).
27. H. Raether, *Surface Plasmons on Smooth and Rough Surfaces and on Grating* (Springer, 1988).
28. S. Maier, *Plasmonics: Fundamentals and Applications* (Springer, 2007).
29. W. L. Barnes, A. Dereux, and T. W. Ebbesen, Nature **424**, 824 (2003).
30. E. Ozbay, Science **311**, 189 (2006).
31. Y. J. Bao, B. Zhang, Z. Wu, J. W. Si, M. Wang, R. W. Peng, X. Lu, J. Shao, Z. F. Li, X. P. Hao, and N. B. Ming, Appl. Phys. Lett. **90**, 251914 (2007).
32. Z. J. Zhang, R. W. Peng, Z. Wang, F. Gao, X. R. Huang, W. H. Sun, Q. J. Wang, and M. Wang, Appl. Phys. Lett. **93**, 171110 (2008).
33. M. L. Brongersma and V. M. Shalaev, Science **328**, 440 (2010).
34. W. Cai, W. Shin, S. Fan, and M. L. Brongersma, Adv. Mater. **22**, 5120 (2010).
35. Q. Hu, D. H. Xu, Y. Zhou, R. W. Peng, R. H. Fan, N. X. Fang, Q. J. Wang, X. R. Huang, and M. Wang, Sci. Rep. **3**, 3095 (2013).
36. K. C. Y. Huang, M. K. Seo, T. Sarmiento, Y. J. Huo, J. S. Harris, and M. L. Brongersma, Nat. Photonics **8**, 244 (2014).
37. J. Y. Wang, C. Hu, and J. S. Zhang, Opt. Express **22**, 22753 (2014).
38. Y. Q. Yang, Q. Li, and M. Qiu, Sci. Rep. **6**, 19490 (2016).
39. S. Butun, S. Tongay, and K. Aydin, Nano Lett. **15**, 2700 (2015).
40. H. Y. Jeong, U. J. Kim, H. Kim, G. H. Han, H. Lee, M. S. Kim, Y. Jin, T. H. Ly, S. Y. Lee, Y. G. Roh, W. J. Joo, S. W. Hwang, Y. Park, and Y. H. Lee, ACS Nano **10**, 8192 (2016).
41. S. M. Bahauddin, H. Robatjazi, and I. Thomann, ACS Photon. **3**, 853 (2016).
42. W. Liu, B. Lee, C. H. Naylor, H. S. Ee, J. Park, A. T. C. Johnson, and R. Agarwal, Nano Lett. **16**, 1262 (2016).
43. Y. Y. Yang, D. Wang, Z. J. Tan, X. Xiong, M. Wang, R. W. Peng, and N. X. Fang, Opt. Express **25**, 10261 (2017).
44. B. Lee, J. Park, G. H. Han, H. S. Ee, C. H. Naylor, W. J. Liu, A. T. C. Johnson, and R. Agarwal, Nano Lett. **15**, 3646 (2015).
45. K. C. J. Lee, Y. H. Chen, H. Y. Lin, C. C. Cheng, P. Y. Chen, T. Y. Wu, M. H. Shih, K. H. Wei, L. J. Li, and C. W. Chang, Sci. Rep. **5**, 16374 (2015).
46. J. Li, Q. Ji, S. Chu, Y. Zhang, Y. Li, Q. H. Gong, K. H. Liu, and K. Shi, Sci. Rep. **6**, 23626 (2016).
47. Z. Wang, Z. Dong, Y. Gu, Y. H. Chang, L. Zhang, L. J. Li, W. Zhao, G. Eda, W. Zhang, G. Grinblat, S. A. Maier, J. K. W. Yang, C. W. Qiu, and A. T. S. Wee, Nat. Commun. **7**, 11283 (2016).
48. S. Najmaei, A. Mlayah, A. Arbouet, C. Girard, J. Leotin, and J. Lou, ACS Nano **8**, 12682 (2014).
49. S. Zu, B. Li, Y. Gong, Z. Li, P. M. Ajayan, and Z. Y. Fang, Adv. Opt. Mater. **4**, 1463 (2016).
50. Y. Yu, Z. Ji, S. Zu, B. Du, Y. Kang, Z. Li, Z. Zhou, K. Shi, and Z. Y. Fang, Adv. Funct. Mater. **26**, 6394 (2016).
51. Z. Li, Y. Li, T. Han, X. Wang, Y. Yu, B. Tay, Z. Liu, and Z. Y. Fang, ACS Nano **11**, 1165 (2017).
52. H. S. Lee, M. S. Kim, Y. Jin, G. H. Han, Y. H. Lee, and J. Kim, Phys. Rev. Lett. **115**, 226801 (2015).
53. D. Wang, J. N. Li, Y. Zhou, D. H. Xu, X. Xiong, R. W. Peng, and M. Wang, Appl. Phys. Lett. **108**, 053107 (2016).